Electron wavepacket control with elliptically polarized laser light in high harmonic generation from aligned molecules

Yann Mairesse, N. Dudovich, J. Levesque, M. Y. Ivanov, P. B. Corkum, D. M. Villeneuve

New Journal of Physics
The open-access journal for physics

Electron wavepacket control with elliptically polarized laser light in high harmonic generation from aligned molecules

Y Mairesse[1,2,5], N Dudovich[1,3], J Levesque[1,4], M Yu Ivanov[1], P B Corkum[1] and D M Villeneuve[1]

[1] National Research Council of Canada, 100 Sussex Drive, Ottawa, Ontario K1A 0R6, Canada
[2] Centre Lasers Intenses et Applications, Université Bordeaux I, UMR 5107 (CNRS, Bordeaux 1, CEA), 351 Cours de la Libération, 33405 Talence Cedex, France
[3] Department of Physics of Complex Systems, Weizmann Institute of Science, Rehovot 76100, Israel
[4] INRS–Énergie et Matériaux, 1650 boul. Lionel-Boulet, CP 1020, Varennes, Québec, J3X 1S2 Canada
E-mail: yann.mairesse@gmail.com

New Journal of Physics **10** (2008) 025015 (13pp)
Received 22 September 2007
Published 29 February 2008
Online at http://www.njp.org/
doi:10.1088/1367-2630/10/2/025015

Abstract. We study experimentally and theoretically the high harmonic emission from aligned samples of nitrogen and carbon dioxide, in an elliptically polarized laser field. The ellipticity induces a lateral shift of the recombining electron wavepacket in the generation process. We show that this effect, which is well known from high harmonic generation (HHG) in atoms, can be useful to maintain the plane wave approximation in the case of HHG from molecules whose orbitals contain nodal planes. The study of the harmonic signal as a function of molecular alignment also reveals the role of the ellipticity on the recollision angle of the electron wavepacket, which can be used to accurately track the position of resonances in harmonic spectra.

[5] Author to whom any correspondence should be addressed.

Contents

1. Introduction

High harmonic generation (HHG) is a process involving intense femtosecond laser light and gas-phase atoms or molecules [1]–[3]. It produces a coherent [4], collimated beam of XUV radiation that is composed of a train of attosecond pulses [5] continuing over the duration of the laser pulse [6, 7]. Single attosecond pulses have been isolated [8, 9] and used to probe attosecond timescale motion in atoms, e.g. Auger decay [10].

It was recently shown [11] that the process of HHG could be used to form an image of a single electron orbital wavefunction of N_2. The principle of the tomographic reconstruction procedure is based on the semi-classical description of the harmonic generation process as a three-step model [12]. (i) An intense femtosecond laser pulse removes the most weakly bound electron. (ii) The electron is accelerated by the laser field for about half an optical cycle, and then is driven back to the parent ion. (iii) The electron recombines with the parent ion, giving off its energy as an XUV photon. If the probabilities of the first two steps can be calibrated, then the XUV spectrum is determined by the transition dipole matrix element that corresponds to the recombination process. Since a wide range of XUV frequencies is generated, the spectrum multiplexes a number of matrix elements in a single measurement.

The quantum mechanical description of HHG is most commonly given by the strong field approximation (SFA) [13]. In the SFA, some of the bound state wavefunction tunnels through the potential barrier near the peak of the laser field. Once in the continuum, the electron is described by a Volkov wavefunction. When the continuum wavefunction returns to the vicinity of the parent ion, it is well described by a chirped plane wave [14]. This plane wave then interacts with the bound state portion of the wavefunction, leading to an oscillating charge that radiates electromagnetic radiation.

In either picture, the HHG spectrum is proportional to the square of the recombination dipole matrix element $\vec{d}$ between the bound state, $\psi_0(\vec{r})$, and the continuum, $\chi(\vec{r})$ [15]. The continuum wavefunction is taken as a plane wave expansion, $\chi(\vec{r}) = \int a(\varepsilon) e^{i\vec{k}(\varepsilon)\cdot\vec{r}} d\varepsilon$, where $a(\varepsilon)$ is the complex amplitude of the recombining electron wavepacket. The electron kinetic energy ε is related to its wavenumber k by $\varepsilon = k^2/2$ (atomic units are used). The XUV photon

frequency Ω is then given by $\Omega = \varepsilon + I_p$, where I_p is the ionization potential. The XUV emission at frequency Ω is then proportional to the square of the matrix element $\vec{d}(\vec{k}) = \langle \psi_0 | \vec{r} | \vec{k} \rangle$.

It turned out that the choice of N_2 for the first tomographic reconstruction with HHG was fortuitous, in that N_2 is one of only a few molecules whose highest occupied molecular orbitals (HOMO) have σ_g symmetry. Most other molecules have π symmetry and have nodal planes upon which the wavefunction goes to zero. The nodal plane creates a node which persists in the continuum wavefunction, hindering the interpretation of the measurements in terms of a wavefunction.

Using an elliptical laser field for HHG offers an additional degree of freedom compared to linear polarization. HHG in elliptically polarized laser fields has been studied for a long time in atoms [16, 17], and more recently in aligned molecules in the particular cases of parallel and perpendicular alignments [18]. It is well known that by applying a small amount of ellipticity to the polarization state of the femtosecond laser light, the trajectory of the electron can be pushed laterally, reducing its probability of recolliding with the parent ion [16, 17]. In the case of a molecule like C_6H_6 which has conjugated π bonds, the effect of this nodal plane has been seen [19]. In addition, the laser ellipticity can induce a change in the direction of the recolliding electron with respect to its direction of ionization. In atoms, this causes a rotation of the direction of polarization of the harmonics [20]. In molecules, where the harmonic signal is very sensitive to the recollision angle of the electron, additional effects appear, as we will show.

In this paper, we perform a complete experimental and theoretical study of the harmonic emission as a function of ellipticity for various molecular alignments and different orbital symmetries. In the first section, we describe the experimental set-up and present the evolution of the harmonic signal as a function of ellipticity for different molecular alignments. We discuss the effects of the width of the recolliding wavepacket and of the recollision angle. In the second section, we present a theoretical model of the harmonic emission in the plane wave approximation and compare it to the experimental results.

2. Ellipticity dependence of harmonic spectra

2.1. Experimental set-up

The experimental set-up has been described previously [11, 21]. Briefly, N_2 or CO_2 gas was introduced into the vacuum chamber through a pulsed supersonic valve providing a gas density of about $10^{17}\,\mathrm{cm}^{-3}$ with a rotational temperature of about 30 K. A 30 fs duration, 800 nm laser pulse with an intensity of about $5 \times 10^{13}\,\mathrm{W\,cm}^{-2}$ created a superposition of rotational states, leading to periodic revivals of molecular alignment [22]–[24]. The direction along which the molecular axes were aligned could be rotated by means of a half waveplate. At the peak of the rotational revival, a second, more intense, laser pulse was focused into the gas to produce high harmonics. Its intensity was $\sim 2 \times 10^{14}\,\mathrm{W\,cm}^{-2}$. Its ellipticity was controlled by a fixed quarter waveplate and an adjustable half waveplate. This configuration maintained the major axis of the polarization ellipse in the same direction. The HHG spectra were recorded by an XUV spectrometer consisting of a variable groove spacing grating and an MCP and CCD camera. A reference spectrum from Ar gas was recorded under identical conditions to calibrate the amplitude of the continuum wavefunction [11, 14].

HHG spectra were recorded for molecules aligned in 5° steps in the range of $\pm 100^\circ$ relative to the intense laser's polarization. These measurements were then repeated for ellipticity $\epsilon = E_y/E_x$ in the range ± 0.36.

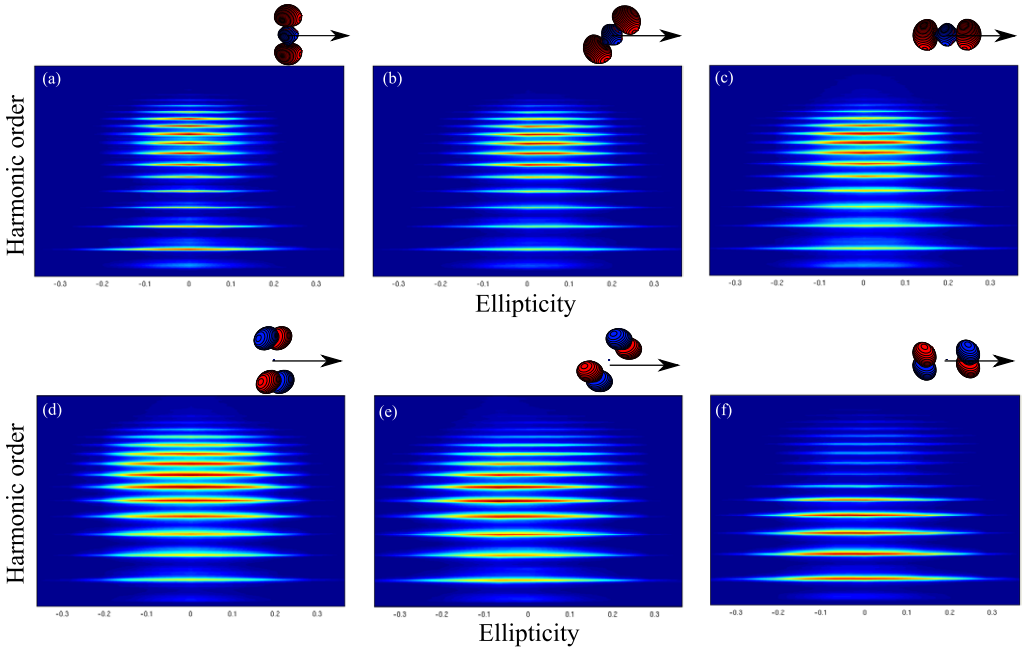

Figure 1. Experimental high harmonic spectra as a function of ellipticity in N_2 (top) and CO_2 (bottom) molecules. The vertical axis is the wavelength axis of the spectrometer, with higher frequency towards the top. The first harmonic is H17. The horizontal axis is the degree of ellipticity $\epsilon = E_y/E_x$ of the generating laser. Each panel corresponds to a different alignment of the molecule with respect to the polarization of the laser field (symbolized by the black arrow on the sketches): -90° ((a) and (d)), -45°((b) and (e)) and 0°((d) and (f)).

2.2. Width of the recolliding wavepacket

Figures 1(a)–(c) present the evolution of the harmonic spectra generated in N_2 as a function of the ellipticity ϵ of the generating laser field, for three molecular alignments. As generally observed in atoms, the harmonic signal is found to decrease as the ellipticity increases. The molecular alignment has a strong influence on the ellipticity dependence of the harmonic emission: the signal decreases faster in perpendicular molecules. Note that we do not observe any dip in the harmonic signal around zero ellipticity, as was previously measured [18]. This is due to the fact that our ellipticity steps are too large in the experiment.

In CO_2 (figures 1(d)–(f)), there is an important difference at parallel alignment between the harmonics below and above H29. This harmonic order corresponds to an amplitude minimum in the harmonic spectrum, which will be discussed later in the paper.

In order to evaluate quantitatively the influence of ellipticity on HHG, we have performed Gaussian fits of the harmonic intensity as a function of ellipticity: $I = I_0 \exp(-\beta(\epsilon - \epsilon_0))^2$. For each molecular alignment and harmonic order, we extract the decay rate β as well as the ellipticity ϵ_0 that maximizes the harmonic signal.

Figure 2(a) shows the extracted decay rate β in N_2. The decay of the harmonic signal as a function of ellipticity is due to the finite lateral extension of the recolliding wavepacket. The decay rate in N_2 increases with the harmonic order for any molecular alignment, as generally observed in atoms [16, 17]. The decay rate is stronger when molecules are perpendicular to the

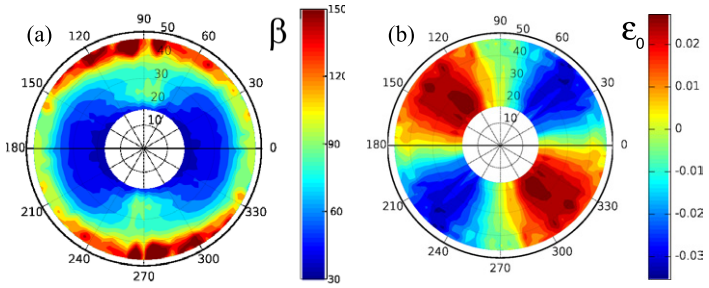

Figure 2. Polar plots of the measured decay rate β (a) and maximizing ellipticity ϵ_0 (b) in N_2. The major axis of the laser polarization is horizontal, and the polar angle is the alignment of the molecule. The radial coordinate is the harmonic order, which increases from 17 to 47 as the radius increases.

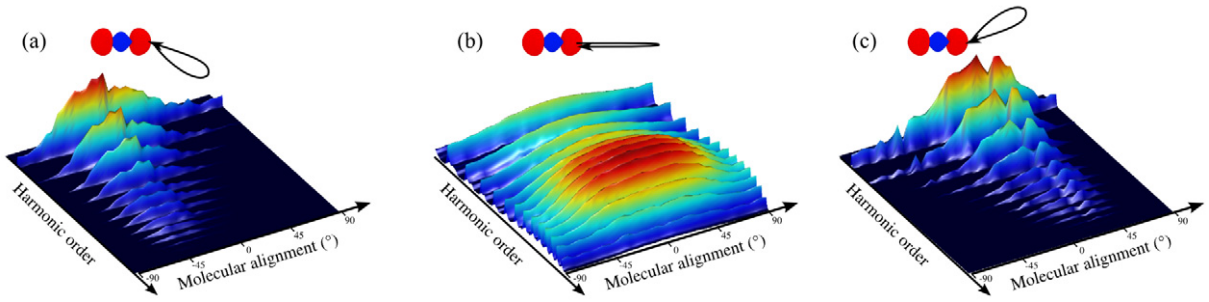

Figure 3. Harmonic spectra as a function of molecular alignment, in N_2. The first harmonic is H17. Each panel corresponds to a fixed laser ellipticity: $\epsilon = -0.29$ for (a), $\epsilon = 0$ for (b) and $\epsilon = 0.29$ for (c).

laser field. This means that the recolliding wavepacket is narrower at perpendicular alignment, and that it was broader at its birth into the continuum. This observation is in agreement with the intuitive picture of tunnel ionization from the HOMO of N_2.

2.3. Influence of the recollision angle

In atomic media, the harmonic signal is always maximum at zero ellipticity. This is not the case in aligned molecules, as shown in figure 2(b). At intermediate alignments, the harmonic signal is maximized by a non-zero ellipticity ϵ_0: when the nitrogen molecules are aligned at -45° of the main axis of the generating laser field, the harmonic signal increases with ellipticity until $\epsilon_0 = 0.03$, where it is maximum. The sign of the maximizing ellipticity ϵ_0 depends on the sign of the angle between the molecule and the laser field.

In order to understand this effect, one must consider the electron trajectories in the elliptical laser field. The electrons that contribute to HHG must have a closed trajectory. They emerge in the continuum with a transverse velocity that compensates for the lateral drift that they acquire in the laser field. Their trajectory is thus not linear, and they come back with a certain angle with respect to the main axis of the laser field polarization. The recollision angle depends on the harmonic order, field strength and ellipticity.

HHG in linear molecules is known to be very sensitive to the angle of the recolliding electron with respect to the molecular axis. Figure 3 shows high harmonic spectra as a

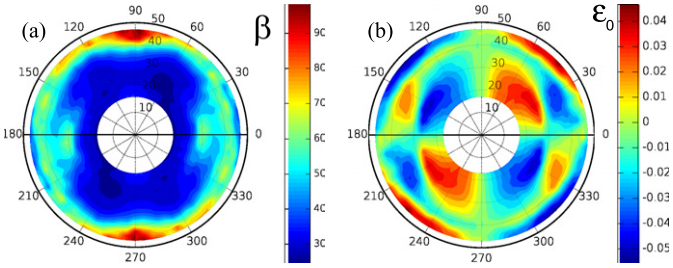

Figure 4. Polar plots of the measured decay rate β (a) and maximizing ellipticity ϵ_0 (b) in CO_2.

function of molecular alignment, in linear and elliptical laser fields. We focus here on the case of nitrogen. Let us consider a N_2 molecule aligned at 45°. With linear polarization, the harmonic signal increases if the molecule is rotated towards the generating laser polarization, i.e. if the recollision direction decreases. If the laser field is elliptical, the recollision direction is modified. For a negative ellipticity, the additional contribution to the recollision angle is negative. Consequently, the recollision angle for our molecule aligned at 45° is more than 45°, and the harmonic signal decreases. The situation is opposite for a positive ellipticity. This explains why the angle at which the harmonic emission is maximum changes as the ellipticity increases (figures 3(a)–(c)).

At a fixed molecular alignment, the harmonic signal from N_2 will increase if the ellipticity decreases the recollision angle, i.e. if it is positive. However if the ellipticity is too strong, the overlap between the recolliding wavepacket and the ground state is poor and the harmonic signal is lowered. The ellipticity ϵ_0 that maximizes the harmonic signal (figure 2(b)) corresponds to a trade off between these two effects.

2.4. Recollision angle and resonances

In CO_2, the situation is more complex, as can be seen in figures 4(a) and (b). Close to parallel alignment, the decay rate β presents a local maximum around H31. An interesting feature also appears on the ϵ_0 map: for a given molecular alignment (close to parallel alignment), the sign of the ellipticity that maximizes the harmonic signal changes at a certain harmonic order. This harmonic order increases as the molecule is rotated away from the laser polarization, from H29 at 10° to H35 at 50°.

In order to explain these results, one must first consider the case of HHG with linear polarization. Figure 5(b) presents the harmonic spectra measured in CO_2 as a function of molecular alignment. For the lowest orders, the harmonic intensity monotonically increases as the molecule is rotated away from the laser polarization. In an elliptical laser field, the harmonic signal will increase if the ellipticity increases the recollision angle of the electron. This is the opposite of what is observed in N_2. This explains why for the lowest harmonics, the sign of the maximizing ellipticity ϵ_0 is opposite in N_2 and CO_2.

For higher orders, the alignment dependence of the harmonic signal is more complex. At parallel alignment, there is a minimum in the harmonic spectrum at H29. As the molecule is rotated away from the laser polarization, the position of this minimum shifts to higher orders. This minimum is due to a resonance between the recolliding electron wavepacket and the orbital, and has been interpreted in terms of two center interference [25]–[27].

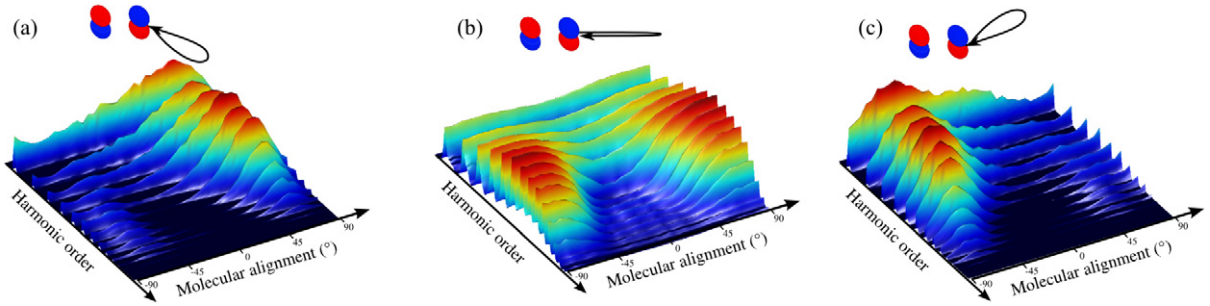

Figure 5. Harmonic spectra as a function of molecular alignment, in CO_2. The first harmonic is H17. Each panel corresponds to a fixed laser ellipticity: $\epsilon = -0.29$ for (a), $\epsilon = 0$ for (b) and $\epsilon = 0.29$ for (c).

Let us examine the behavior of harmonics located above the resonance, e.g. H31. In a linearly polarized laser field, the harmonic intensity decreases as the molecule is rotated away from the laser polarization until the alignment angle reaches 30°. Consequently, in an elliptical laser field, the signal will increase if the ellipticity decreases the recollision angle. For molecular alignments above 30°, the situation is opposite: the signal will increase if the ellipticity increases the recollision angle. This explains why the ellipticity ϵ_0 that maximizes H31 changes sign in figure 4(b) around 30°.

The strong decay rate β measured around H31 at parallel alignment can also be explained by the influence of the recollision angle above the resonance. For a parallel molecule, as the ellipticity increases the signal decreases not only because of the lateral shift of the electron wavepacket, but also because of the increasing recollision angle.

These results show that the laser ellipticity can be used as a parameter to accurately control the recollision angle of the electron wavepacket. The measurements of the maximizing ellipticity ϵ_0 offer a way to precisely map the position of the resonance: the position of the sign change of ϵ_0 is easier to determine than the amplitude minimum on harmonic spectra. This type of control of the recollision angle could be extended to perform tomographic reconstructions of atomic orbitals [28], in which the ability to align in space that molecules provide is not available.

3. Model of molecular high harmonic emission in an elliptical laser field

We now proceed to model the process based on the three-step model [12]. Two important effects have to be present in the model: the transverse dimensions of the recolliding wavepacket, which is set by tunnel ionization, and the recollision angle.

3.1. Tunnel ionization

The ionization step is modeled using a simplified tunnel ionization model [29] which is based on earlier work by Delone and Krainov [30]. This model estimates the distribution of lateral momentum of the electron immediately after tunnel ionization. The probability of a lateral momentum $p_\perp$ is given by

$$P(p_\perp) = \mathrm{e}^{-p_\perp^2 \tau/2},$$

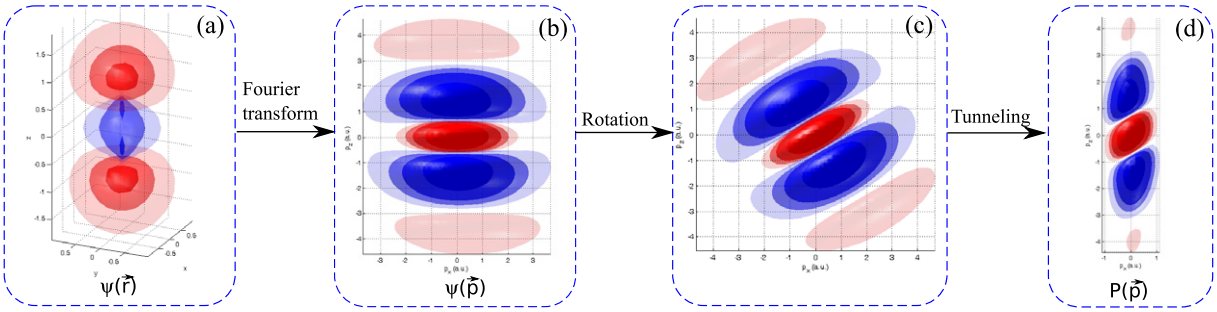

Figure 6. Calculation of the electron wavepacket momentum distribution at its birth in the continuum. (a) Three-dimensional (3D) plot of the $3\sigma_g$ HOMO wavefunction of N_2, $\psi(\vec{r})$, in coordinate space, as calculated by GAMESS. The z-axis corresponds to the molecular axis. (b) HOMO wavefunction of N_2, $\psi(\vec{p})$, in momentum space. This is the spatial Fourier transform of (a). (c) $\psi(\vec{p})$, in momentum space, after it has been rotated by an angle of 30° (by applying a rotation matrix). (c) Rotated HOMO wavefunction of N_2, $\psi(\vec{p})$, multiplied by the tunneling filter function.

where $\tau = \Gamma/\omega$ is the tunneling time, $\Gamma = 4I_p\omega^2/E$ is the Keldysh parameter, ω is the laser angular frequency, I_p is the ionization potential, and E is the laser electric field.

The distribution of lateral momenta before tunneling is given as the spatial Fourier transform of the orbital wavefunction rotated by angle θ in the laboratory frame. We illustrate this procedure in the following steps. Figure 6(a) shows $\psi(\vec{r})$, the HOMO of N_2 calculated using GAMESS [31], with the z-axis being the molecular axis. Figure 6(b) shows the spatial Fourier transform of the HOMO, $\psi(\vec{p})$. The momentum-space wavefunction is then rotated to represent the orientation of the molecule relative to the laser polarization (figure 6(c)).

The rotated momentum representation of the wavefunction is multiplied by the lateral width of the tunnel as described above, to represent tunneling along the z-axis. The result is shown in figure 6(d). Finally, we integrate the function in the positive z-direction to include all momentum components that are traveling in the direction of the laser field. This results in a 2D function $P(p_x, p_y)$ that represents the probability of a particular lateral momentum component tunneling from that orbital wavefunction for the molecule rotated at an angle θ. The lateral momentum probability that we have illustrated is written as

$$P(p_x, p_y) = \int_0^\infty |\psi(p_x, p_y, p_z; \theta)|^2 \, \mathrm{e}^{-(p_x^2+p_y^2)\tau/2} \, \mathrm{d}p_z.$$

These probability distributions $P(p_x, p_y)$ can be integrated to yield an estimate of the total probability of ionization at each molecular angle. These angle-dependent ionization probabilities are shown in figure 7. The molecular axis is horizontal. These should be compared with the prediction of the MO–ADK model of molecular ionization [32]. The overall features are similar, although the present model tends to overestimate the rate near 90°. This is because the molecule is elongated when viewed from 90°, and the Δx is large, leading to a smaller Δp from the uncertainty principle. Thus more of the wavefunction can pass through the tunnel filter.

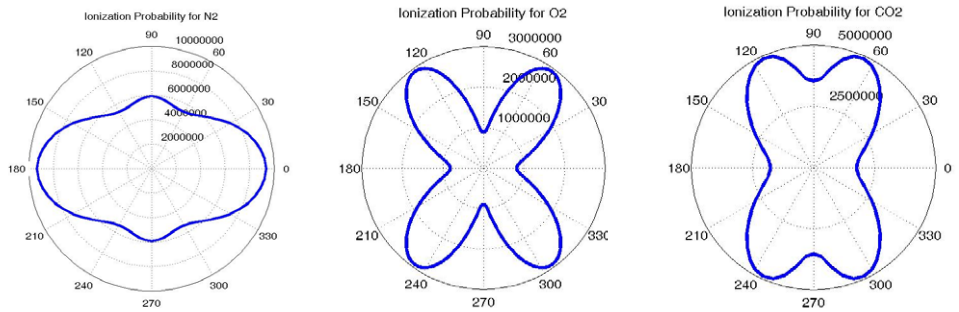

Figure 7. Integrated tunnel ionization momentum distributions versus molecular angle for N_2, O_2 and CO_2. These values correspond approximately to the molecular ADK calculations.

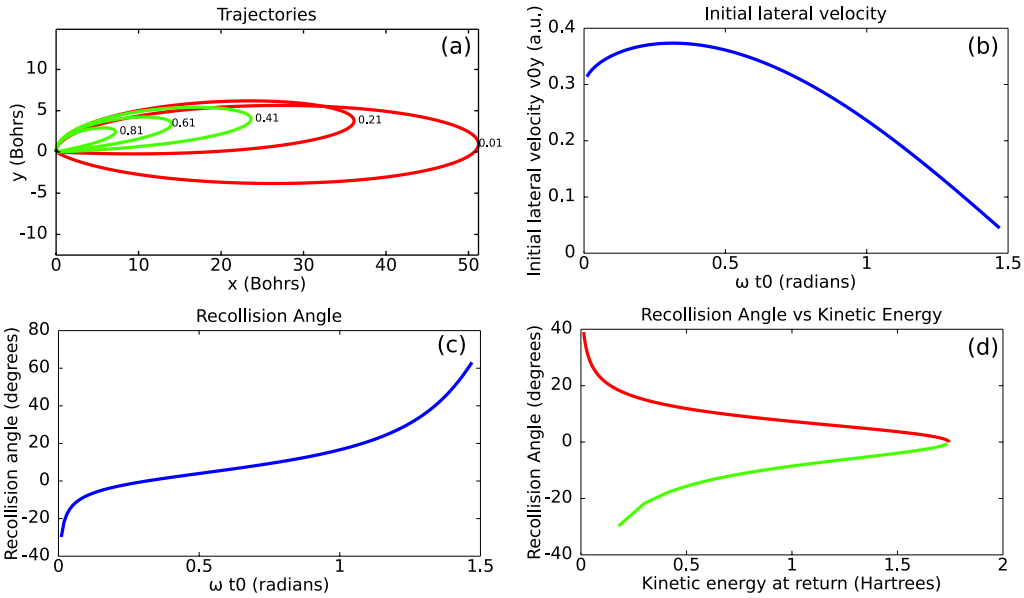

Figure 8. Classical trajectories of electrons between the instants of ionization and recollision with a parent atom for an ellipticity of 0.1 and a laser intensity of 2.5×10^{14} W cm^{-2}. The label on each trajectory is the optical phase of ionization in radians. Each trajectory starts in the north-east direction. The short trajectories are in green and the long trajectories in red. (b) Initial lateral velocity required in order to make the trajectory recollide with the parent, as a function of phase of ionization. (c) Angle with which the electron recollides with the parent, as a function of phase of ionization. (d) Recollision angle as a function of the return kinetic energy of the electron, for the short (green) and long (red) trajectories.

3.2. Recollision angle

The next step of the model is to calculate the classical trajectories of electrons between the time that they are ionized in the intense field and the moment that they recollide with the parent. For a given time of ionization and a given ellipticity, the condition of recollision determines the value of the initial lateral momentum that is required. Figure 8(a) shows some sample trajectories for

a set of initial phases. The phase $\omega t_0 = 0.3$ corresponds to the highest kinetic energy of return ($3.17U_p$), and separates the long trajectories ($\omega t_0 < 0.3$) from the short trajectories ($\omega t_0 > 0.3$). It is remarkable that the sign of the recollision angle is opposite for these two families of trajectories.

The classical trajectories can be used to determine the value of the initial lateral momentum that is required to ensure recollision. This determines the function $p_\perp(\epsilon, t_0)$, shown in figure 8(b). Similarly, the angle at which the electron recollides relative to the laser polarization is given by the function $\theta_{\text{recoll}}(\epsilon, t_0)$, also shown in figure 8(c). We also calculate the kinetic energy K with which the electron returns to the parent. As can be seen in figure 8(d), the recollision angles for the short and long trajectories are almost opposite.

3.3. Results

We are now prepared to put the preceding calculations together, in order to calculate our theoretical prediction of the HHG spectra of aligned molecules in elliptically polarized light. We proceed as follows:

1. For each ellipticity ϵ, molecular angle θ and kinetic energy of the recolliding electron K, do the following.
2. Find the lateral momentum $p_\perp$ required for recollision.
3. Find the probability of this momentum from the tunneling calculation.
4. Find the recollision angle θ_{recoll}. This is used to rotate the molecular orbital into the frame of the returning electron.
5. Calculate the transition dipole matrix element between the molecular orbital and the recolliding electron plane wave with energy K.
6. Calculate the product of the square of the transition dipole and the ionization probability.
7. The last item is plotted versus all three parameters.

We show the results of this model in figure 9, along with the experimental measurements. The experimental curves have been divided by the argon reference [11] to remove experimental details. Although the details of the HHG spectrum for $\epsilon = 0$ and $\theta = 0$ differ, the agreement becomes better for increasing ellipticity.

The calculation has been repeated for CO_2, and is shown in figure 10. Here we do not expect good agreement for $\epsilon = 0$ due to the presence of the nodal plane in the HOMO. CO_2's nodal plane violates the assumption of the model, that the recolliding electron can be described by a plane wave. However as the ellipticity increases, the agreement between the experiment and the theory becomes better. For the strongest ellipticity (-0.29) the experimental signal is maximum when molecules are aligned around 120° while the theoretical results show a maximum around 105°. Interestingly, the secondary maximum observed in the simulations around 45° is present in the experimental data, but shifted around 60°. This means that at strong ellipticity the plane wave approximation successfully describes the experimental results: the nodal plane is pushed away and the recolliding wavepacket is a plane wave.

4. Conclusion

The use of an elliptical laser field for HHG from aligned molecules offers new possibilities of control and characterization of the generation process.

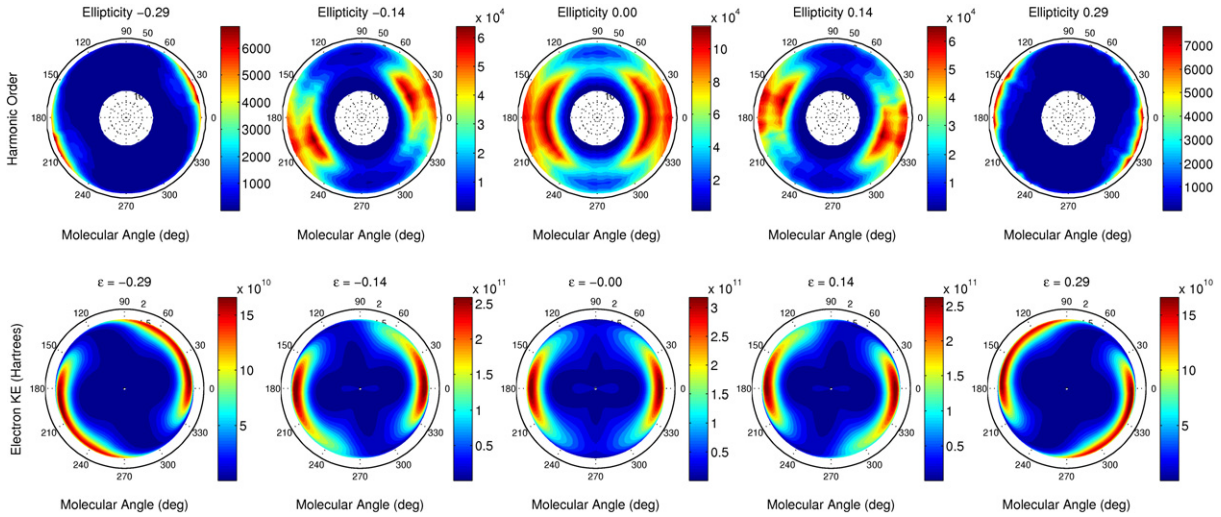

Figure 9. Top row: experimentally measured HHG spectra for N_2 molecules aligned at various angles relative to the laser polarization, for five ellipticities. These values have been divided by the argon reference. Bottom row: predictions of the model for the same conditions.

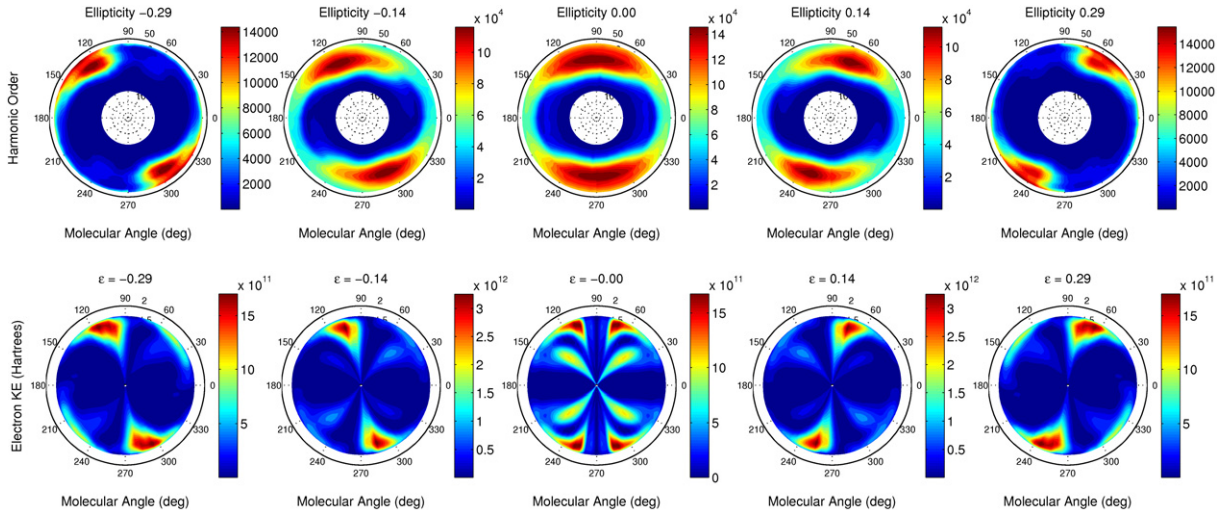

Figure 10. Top row: experimentally measured HHG spectra for CO_2 molecules aligned at various angles relative to the laser polarization, for five ellipticities. These values have been divided by the argon reference. Bottom row: predictions of the model for the same conditions.

In the first section, we have shown that a small ellipticity can induce slight changes of the recollision angle. This effect can be utilized to determine accurately the position of amplitude minima associated with resonances in the harmonic spectra. More generally, the ellipticity can be used as a perturbation to measure precisely the effect of the recollision angle on harmonic generation.

In the second section, we have developed a theoretical model of harmonic emission in an elliptical laser field in the plane wave approximation. We believe that the agreement between this model and the experiment for non-zero ellipticities shows that we can use the plane wave approximation to model the process of HHG from aligned molecules with elliptically polarized laser fields. If the elliptically polarized light succeeds in pushing the nodal plane of the wavefunction sideways, so that the recolliding wavepacket can be written as a plane wave, then it is possible to tomographically reconstruct the wavefunction using the already established algorithm [11]. This is a general procedure that should be applicable to many molecules which have nodal planes. This will open up the technique of molecular orbital tomography to a larger set of molecules.

References

[1] Rosman R, Gibson G, Boyer K, Jara H, Luk T S, McIntyre I A, McPherson A, Solem J C and Rhodes C K 1988 *J. Opt. Soc. Am.* B **5** 1237
[2] L'Huillier A and Balcou P 1993 *Phys. Rev. Lett.* **70** 774
[3] L'Huillier A, Descamps D, Johansson A, Norin J, Mauritsson J and Wahlström C-G 2003 *Eur. Phys. J.* D **26** 91
[4] Lyngå C, Gaarde M B, Delfin C, Bellini M, Hänsch T W, L Huillier A and Wahlström C-G 1999 *Phys. Rev.* A **60** 4823
[5] Scrinzi A, Ivanov M Y, Kienberger R and Villeneuve D M 2006 *J. Phys. B: At. Mol. Opt. Phys.* **39** R1
[6] Paul P M, Toma E S, Breger P, Mullot G, Balcou F A P, Muller H G and Agostini P 2001 *Science* **292** 1689
[7] Mairesse Y *et al* 2003 *Science* **302** 1540
[8] Hentschel M, Kienberger R, Spielmann C, Reider G A, Milosevic N, Brabec T, Corkum P, Heinzmann U, Drescher M and Krausz F 2001 *Nature* **414** 509
[9] Sola I J *et al* 2006 *Nat. Phys.* **2** 319
[10] Drescher M, Hentschel M, Kienberger R, Uiberacker M, Yakovlev V, Scrinzi A, Westerwalbesloh T, Kleineberg U, Heinzmann U and Krausz F 2002 *Nature* **419** 803
[11] Itatani J, Levesque J, Zeidler D, Niikura H, Pépin H, Kieffer J C, Corkum P B and Villeneuve D M 2004 *Nature* **432** 867
[12] Corkum P B 1993 *Phys. Rev. Lett* **71** 1994
[13] Lewenstein M, Balcou P, Ivanov M Y, L'Huillier A and Corkum P B 1994 *Phys. Rev.* A **49** 2117
[14] Levesque J, Zeidler D, Marangos J P, Corkum P B and Villeneuve D M 2007 *Phys. Rev. Lett.* **98** 183903
[15] Bethe H A and Salpeter E E 1957 *Quantum Mechanics of One- and Two-Electron Atoms* (Berlin: Springer)
[16] Budil K S, Salieres P, Perry M D and L'Huillier A 1993 *Phys. Rev.* A **48** R3437
[17] Dietrich P, Burnett N H, Ivanov M and Corkum P B 1994 *Phys. Rev.* A **50** R3585
[18] Kanai T, Minemoto S and Sakai H 2007 *Phys. Rev. Lett.* **98** 053002
[19] Bhardwaj V R, Rayner D M, Villeneuve D M and Corkum P B 2001 *Phys. Rev. Lett.* **87** 253003
[20] Antoine P, Carré B, L'Huillier A and Lewenstein M 1997 *Phys. Rev.* A **55** 1314
[21] Itatani J, Zeidler D, Levesque J, Niikura H, Villeneuve D M and Corkum P B 2005 *Phys. Rev. Lett.* **94** 123902
[22] Sakai H, Safvan C P, Larsen J J, Hilligs K M, Hald K and Stapelfeldt H 1999 *J. Chem. Phys* **110** 10235
[23] Rosca-Pruna F, Springate E, Oerhaus H L, Krishnamurthy M, Farid N, Nicole C and Vrakking M J J 2001 *J. Phys. B: At. Mol. Opt. Phys.* **34** 4919
[24] Dooley P W, Litvinyuk I V, Lee K F, Rayner D M, Spanner M, Villeneuve D M and Corkum P B 2003 *Phys. Rev.* A **68** 23406
[25] Lein M, Hay N, Velotta R, Marangos J and Knight P 2002 *Phys. Rev.* A **66** 023805
[26] Vozzi C *et al* 2005 *Phys. Rev. Lett.* **95** 153902

[27] Kanai T, Minemoto S and Sakai H 2005 *Nature* **435** 470
[28] Kitzler M and Lezius M 2005 *Phys. Rev. Lett.* **95** 253001
[29] Ivanov M Y, Spanner M and Smirnova O 2005 *J. Mod. Opt.* **94** 123902
[30] Delone N B and Krainov V P 1991 *J. Opt. Soc. Am.* B **8** 1207
[31] Schmidt M W *et al* 1993 *J. Comput. Chem.* **14** 1347
[32] Tong X M, Zhao Z X and Lin C D 2002 *Phys. Rev.* A **66** 033402